HHS Public Access

Author manuscript

Sci Signal. Author manuscript; available in PMC 2016 February 26.

Published in final edited form as:

Sci Signal. ; 8(389): ra79. doi:10.1126/scisignal.aaa2581.

HDL-bound sphingosine 1-phosphate acts as a biased agonist for the endothelial cell receptor $S1P_1$ to limit vascular inflammation

Sylvain Galvani[1], **Marie Sanson**[1], **Victoria A. Blaho**[1], **Steven L. Swendeman**[1], **Hideru Obinata**[1,*], **Heather Conger**[2], **Björn Dahlbäck**[3], **Mari Kono**[4], **Richard L. Proia**[4], **Jonathan D. Smith**[2], and **Timothy Hla**[1,†]

[1]Center for Vascular Biology, Department of Pathology and Laboratory Medicine, Weill Cornell Medical College, Cornell University, New York, NY 10065, USA

[2]Department of Cellular and Molecular Medicine, Cleveland Clinic Lerner Research Institute, Cleveland, OH 44195, USA

[3]Department of Translational Medicine, Skåne University Hospital, Lund University, 214 28 Malmö, Sweden

[4]Genetics of Development and Disease Branch, National Institute of Diabetes and Digestive and Kidney Diseases, National Institutes of Health, Bethesda, MD 20892, USA

Abstract

The sphingosine 1-phosphate receptor 1 ($S1P_1$) is abundant in endothelial cells, where it regulates vascular development and microvascular barrier function. In investigating the role of endothelial cell $S1P_1$ in adult mice, we found that the endothelial $S1P_1$ signal was enhanced in regions of the arterial vasculature experiencing inflammation. The abundance of proinflammatory adhesion

†Corresponding author. tih2002@med.cornell.edu.
*Present address: Gunma University, Gunma, 371-8510 Japan.

SUPPLEMENTARY MATERIALS

www.sciencesignaling.org/cgi/content/full/8/389/ra79/DC1

Fig. S1. $S1P_1$ localization in en face preparations of the mouse aorta.
Fig. S2. ICAM-1 and VCAM-1 abundance in aorta upon $S1P_1$ deletion.
Fig. S3. Effect of albumin and albumin-S1P on TNFα-induced increases in ICAM-1 and VCAM-1 abundance.
Fig. S4. Characterization of the sphingolipid composition of human HDL.
Fig. S5. Effect of S1P carrier on $S1P_1$ retention at the cell surface.
Fig. S6. Effect of $S1P_1$ inhibition in S1P-induced activation of MAPK.
Fig. S7. Subcellular localization of β-arrestin 2 depends on the S1P carrier.
Fig. S8. Genetic modulation of $S1P_1$ expression in endothelial cells and modification of ICAM-1 abundance.
Fig. S9. Analysis of weight, plasma cholesterol, and cell populations in $Apoe^{-/-}$ *S1pr1* wild-type and ECKO animals after 16 weeks on a high-fat diet.
Fig. S10. Plasma sphingolipid characterization.
Fig. S11. Analysis of plaque composition.
Fig. S12. Atherosclerotic root lesion quantification.

Author contribution: S.G. designed the studies, carried out most of the experiments, and analyzed the data. M.S. helped in the generation of $Apoe^{-/-}$ *S1pr1* mutant mice. V.A.B. performed flow cytometry analysis on blood from $Apoe^{-/-}$ *S1pr1* mutant animals. S.L.S. prepared and characterized mice HDL. H.O. constructed the lentiviral vectors used in this study. H.C. performed the aortic root Oil Red O staining and the root atherosclerotic plaque analysis. B.D., R.L.P., M.K., and J.D.S. provided conceptual input and critical reagents. T.H. provided conceptual input, supervised the study, and wrote the manuscript with S.G.

Competing interests: The authors declare that they have no competing interests.

proteins, such as ICAM-1, was enhanced in mice with endothelial cell–specific deletion of *S1pr1* and suppressed in mice with endothelial cell–specific overexpression of *S1pr1*, suggesting a protective function of $S1P_1$ in vascular disease. The chaperones $ApoM^+$HDL (HDL) or albumin bind to sphingosine 1-phosphate (S1P) in the circulation; therefore, we tested the effects of S1P bound to each chaperone on $S1P_1$ signaling in cultured human umbilical vein endothelial cells (HUVECs). Exposure of HUVECs to $ApoM^+$HDL-S1P, but not to albumin-S1P, promoted the formation of a cell surface $S1P_1$–β-arrestin 2 complex and attenuated the ability of the proinflammatory cytokine TNFα to activate NF-κB and increase ICAM-1 abundance. Although S1P bound to either chaperone induced MAPK activation, albumin-S1P triggered greater G_i activation and receptor endocytosis. Endothelial cell–specific deletion of *S1pr1* in the hypercholesterolemic *Apoe*$^{-/-}$ mouse model of atherosclerosis enhanced atherosclerotic lesion formation in the descending aorta. We propose that the ability of $ApoM^+$HDL to act as a biased agonist on $S1P_1$ inhibits vascular inflammation, which may partially explain the cardiovascular protective functions of HDL.

INTRODUCTION

Vascular inflammation and endothelial dysfunction represent early events in cardiovascular disease (1). During vascular inflammation, endothelial function is altered, characterized by impaired nitric oxide release and an increase in the abundance of leukocyte adhesion molecules such as intercellular adhesion molecule–1 (ICAM-1) and vascular cell adhesion molecule–1 (VCAM-1), leading to the recruitment of proinflammatory immune cells into the vascular wall (2). Endothelial inflammation is affected by hemodynamic shear forces. In the descending aorta, laminar shear forces promote endothelial cell alignment, which suppresses inflammation. In contrast, in the aortic arch, the lesser curvature, and the branch points, turbulent flow induces random alignment of cells and vascular inflammation. Such regions are prone to atherosclerotic plaque formation (3). Plasma lipoproteins play a crucial role for either protection from or promotion of atherosclerosis (4). Indeed, altered concentrations of high-density lipoprotein (HDL) and low-density lipoprotein (LDL) represent a well-established risk factor for cardiovascular disease. High plasma concentrations of LDL injures the endothelium and promotes vascular inflammation (5, 6), whereas HDL is protective, partially by promoting endothelial function (7). Although the atheroprotective effect of HDL was initially attributed primarily to cholesterol removal from tissues, anti-inflammatory and endothelial protective functions of HDL may also be important (8). HDL particles are composed of apolipoproteins (such as ApoA-I, ApoA-II, and ApoM), enzymes involved in antioxidative mechanisms such as paraoxonase-1, lecithin-cholesterol acyltransferase, and diverse lipid species, including cholesterol esters, triglycerides, phospholipids (9), and bioactive sphingolipids such as sphingosine 1-phosphate (S1P) (10).

S1P is a lipid mediator that regulates many physiologic functions, especially those in the vascular and immune systems (11–13). It is concentrated in plasma (~1 μM) and carried primarily by the $ApoM^+$ subfraction of HDL (~65%; $ApoM^+$HDL) (14), with the remainder bound to plasma albumin (~35%). S1P signals through specific G protein (heterotrimeric guanine nucleotide–binding protein)–coupled receptors (GPCRs) [sphingosine 1-phosphate

receptors 1 to 5 ($S1P_{1–5}$)] and regulates various cellular responses. In particular, $S1P_1$ inhibits vascular permeability and is required for vascular development (15) as well as immune cell trafficking. Moreover, a functional antagonist of $S1P_1$ (fingolimod/Gilenya) has been approved to treat relapsing-remitting multiple sclerosis (16). $S1P_1$ is abundant in endothelial cells and is critical for laminar shear stress signaling and stabilization of the nascent vascular network (17). The ability of various chaperones to modify the functions of S1P is not well understood.

The role of the $S1P_1$ receptor in vascular pathology is unclear. In nonobese diabetic (NOD) mice, $S1P_1$ is an anti-inflammatory receptor, its stimulation leads to reduced adhesion of monocytes to endothelial cells (18). In addition, $S1P_1$ stimulation in macrophages promotes an anti-inflammatory M2-like phenotype in vitro (19). In vivo, pharmacological agents (KRP203, an $S1P_1$-specific agonist, or FTY720, which targets all S1P receptors except $S1P_2$) attenuate atherosclerotic plaque development in *Ldlr*$^{-/-}$ and *Apoe*$^{-/-}$ mouse models (20–22). In contrast, stimulation of endothelial cells with S1P increases the surface abundance of adhesion molecules (VCAM-1 and ICAM-1), although it inhibits tumor necrosis factor–α (TNFα)–induced increases in the abundance of these molecules (23, 24). This inhibitory effect has been ascribed to $S1P_1$ and/or $S1P_3$ stimulation (24, 25). Additionally, S1P cooperates with lipopolysaccharide and induced inflammatory molecules and leukocyte adhesion on endothelial cells in vitro (26). These somewhat disparate findings underscore the need to clarify the role of this abundant lipid mediator in vascular inflammation and atherosclerosis.

Here, we report that mouse endothelial $S1P_1$ acted as an anti-inflammatory and anti-atherosclerotic GPCR in vivo. In addition, $ApoM^+$HDL engaged human endothelial $S1P_1$ to form an anti-inflammatory signaling complex with β-arrestin 2 that suppressed nuclear factor κB (NF-κB)–dependent inflammatory pathways. Collectively, these data suggest that S1P bound to the chaperone $ApoM^+$HDL activates the endothelial $S1P_1$ GPCR as a biased agonist to suppress inflammatory responses and atherosclerosis.

RESULTS

$S1P_1$ is differentially activated along the aortic endothelium

We have shown (17) that $S1P_1$ is localized on the plasma membrane in the descending aorta. In contrast, in the lesser curvature, $S1P_1$ is intracellular and colocalized with endosomal markers (17) (fig. S1A). The abundance of the proinflammatory cell adhesion molecules, ICAM-1 and VCAM-1 (fig. S1, B and C), was increased in the lesser curvature compared to the descending aorta. To study the role of $S1P_1$ signaling and its role in inflammation, we used the $S1P_1$ reporter mice [$S1P_1$–green fluorescent protein (GFP) reporter mice] (27). In these mice, endogenous activation of $S1P_1$ leads to the recruitment of a β-arrestin/TEV (tobacco etch virus) protease fusion protein, resulting in the release of a transcription factor that stimulates the expression of nuclear-localized GFP reporter. In the lesser curvature, subclavian-carotid bifurcation, thoracic branching point, and aortic valves (Fig. 1), substantial numbers of endothelial cells had nuclear GFP, suggesting an increase of $S1P_1$ signaling. In contrast, nuclear GFP was not detected in the regions of the aortic tree exposed to laminar shear stress such as medial aspect of the carotid branch point or descending aorta

(Fig. 1). These results suggest a correlation between disturbed shear forces, inflammation, and exaggerated $S1P_1$ signaling/internalization.

Endothelial *S1pr1* expression suppresses vascular inflammation

To study the role of endothelial $S1P_1$ in vascular inflammation, we used the endothelial cell–specific inducible knockout mouse line (*S1pr1*$^{f/f}$ *Cdh5-Cre*^{ERT2}, referred to as *S1pr1ECKO*) (17) and deleted endothelial *S1pr1* at 4 weeks of age. Efficiency of deletion has been previously assessed by quantitative reverse transcription polymerase chain reaction analysis of endothelial cells isolated from lung tissue (17) as well as by immunofluorescence of the aortic tissue (Fig. 2A), which displayed an almost complete loss of $S1P_1$ immunofluorescence in the aortic endothelium. We did not detect differences in vascular endothelial (VE)–cadherin immunofluorescence between wild-type and *S1pr1ECKO* aortic endothelium. However, *S1pr1ECKO* aorta showed an increase in VCAM-1 and ICAM-1 immunofluorescence (Fig. 2, B and C), especially in the descending aorta.

To further validate the anti-inflammatory effect of $S1P_1$, we immunoblotted dissected aortic extracts for ICAM-1 and VCAM-1. The abundance of ICAM-1 and to a lesser extent that of VCAM-1 was significantly increased in *S1pr1ECKO* aortae compared to control, especially in the descending aorta (fig. S2, A and B). Cell surface biotinylation assays of excised aortae showed increased ICAM-I abundance at the surface of *S1pr1ECKO* aorta (fig. S2C). Together, these results suggested that deletion of *S1pr1* in endothelial cells promoted a proinflammatory state in the aortic endothelium.

To further confirm the involvement of $S1P_1$ in the control of vascular inflammation, we next used the inducible endothelial-specific $S1P_1$ overexpression mouse line (*S1pr1*$^{f/stop/f}$ *Cdh5-Cre*^{ERT2}, referred to as $S1P_1$ ECGOF) (17). Overexpression of endothelial *S1pr1* was induced at 4 weeks of age. Efficiency of the overexpression was assessed by immunofluorescence of the aortic tissue (Fig. 2D), which showed a strong, albeit mosaic increase in $S1P_1$ staining. Overexpression of $S1P_1$ in the vascular endothelium led to increased membrane localization of $S1P_1$ in the lesser curvature of *S1pr1ECGOF* aorta. Similar to *S1pr1ECKO* aorta, we did not detect substantial differences in VE-cadherin staining. In contrast, *S1pr1ECGOF* animals showed a decrease in ICAM-1 staining (Fig. 2E) in both lesser curvature and descending aorta, suggesting that $S1P_1$ suppressed endothelial inflammatory gene expression.

HDL-bound S1P attenuates cytokine-induced increases in adhesion molecule abundance in endothelial cells

On the basis of the anti-inflammatory properties of endothelial $S1P_1$ in vivo, we hypothesized that $S1P_1$ induces an anti-inflammatory signal in endothelial cells. In human umbilical vein endothelial cells (HUVECs) treated with the proinflammatory cytokine TNFα, ICAM-1 abundance increased in a time-dependent fashion, a response that was attenuated (~70%) by co-incubation with HDL from wild-type mice ($ApoM^+$ HDL) (Fig. 3, A and B). HDL particles contained ~4.79 ± 0.975 pmol S1P per microgram of protein, as determined by liquid chromatography–tandem mass spectrometry. We estimated the ApoM concentration in HDL preparations to be ~160 ng/μg protein. Thus, under our experimental

conditions, HUVECs were exposed to ~1.5 to 2 μM S1P and ~2.5 μM ApoM. In contrast, HDL isolated from *Apom*$^{-/-}$ mice (ApoM^{-}HDL) did not significantly suppress the TNFα-induced increase in ICAM-1 expression. These HDL particles do not contain detectable ApoM and had very low S1P concentrations (0.038 ± 0.008 pmol S1P/μg protein). Albumin-S1P did not suppress the TNFα-induced increase in ICAM-1 abundance to the same extent as HDLS1P (Fig. 3, A and B). These results suggest that the anti-inflammatory effect of S1P depended on its association with ApoM^{+}HDL. Dose-response analysis of HDL isolated from wild-type and *Apom*$^{-/-}$ mice (Fig. 3, C and D) and albumin-S1P (fig. S3, A and B) further illustrated that the TNFα-induced increase in ICAM-1 abundance was inhibited in a dose-dependent manner by ApoM^{+}HDL but not by ApoM^{-}HDL particles or albumin-S1P. Flow cytometry revealed that VCAM-1 abundance was increased by TNFα treatment (fig. S3C), a response that was partially suppressed (~40%) by S1P bound to recombinant ApoM but not by recombinant ApoM alone, and to a lesser extent by albumin-bound S1P (~20%) (fig. S3C). Together, these data suggest that S1P bound to ApoMin HDL particles potently suppressed cytokine-induced increases in adhesion molecule abundance in endothelial cells.

Cytokine-induced NF-κB activation is attenuated by HDL-bound S1P

The NF-κB pathway is a key inflammatory signaling pathway induced by TNFα in endothelial cells, and its activation requires the phosphorylation of the p65 NF-κB subunit (28). TNFα stimulation of HUVECs increased the phosphorylation of p65 within 10 min, a response that was suppressed by co-incubation with human HDL (fig. S4) in a dose-dependent manner (Fig. 4, A and B). Similarly, HDL isolated from wild-type mice (ApoM^{+}HDL) inhibited the phosphorylation of p65 in a dose-dependent manner, whereas ApoM^{-}HDL was less effective (Fig. 4, C and D). These observations suggest that S1P bound to HDL antagonized the cytokine-induced NF-κBpathway in endothelial cells.

HDL-S1P induces the persistent presence of $S1P_1$ at the cell membrane

HDL-S1P enhances endothelial barrier function by activating $S1P_1$ at the cell membrane (29).We investigated the localization of $S1P_1$ in HUVECs expressing GFP-tagged $S1P_1$ (14) and stimulated with various chaperonebound forms of S1P. GFP-tagged $S1P_1$ was localized at the cell membrane under basal conditions, which was not affected by TNFα stimulation or HDL treatment. In contrast, stimulation with albumin-S1P or exposure to P-FTY720 induced receptor endocytosis (Fig. 5A). Cell surface biotinylation assays (fig. S5, A and B) confirmed that albumin- S1P and P-FTY720, but not HDL treatment, induced the disappearance of membrane $S1P_1$. These results suggested that HDLS1P activation of endothelial cells promoted cell surface $S1P_1$, whereas albumin-S1P promotes rapid endocytosis of $S1P_1$.

Cellular responses to S1P are chaperone-dependent

Activation of $S1P_1$ by its ligand S1P leads to G_i-dependent signaling, which activates the mitogen-activated protein kinase (MAPK) extracellular signal–regulated kinase (ERK) and inhibits adenylate cyclase (30). Both albumin-S1P and HDL-S1P induced rapid phosphorylation of ERK [Fig. 5B and (14)], in an $S1P_1$-dependent manner (fig. S6). In contrast, forskolin-activated increases in cyclic adenosine 3′,5′-monophosphate (cAMP)

concentrations were inhibited by albumin-S1P, but not by HDL-S1P (Fig. 5C), suggesting that HDL-S1P acts as a biased agonist for $S1P_1$.

β-Arrestin 2 plays a crucial role in HDL-induced $S1P_1$ anti-inflammatory signaling

After ligand stimulation, β-arrestins associate with GPCRs to promote desensitization and endocytosis (31, 32). β-Arrestins also provide an additional GPCR signaling platform in addition to the heterotrimeric G protein–regulated mechanisms (32, 33), leading to the activation of intracellular signaling responses including the inhibition of the NF-κB pathway (34, 35). We therefore asked whether β-arrestin was involved in mediating endothelial cell anti-inflammatory pathways.

HDL, but not albumin-S1P, treatment increased the association of $S1P_1$ with β-arrestin 2 (Fig. 6A). In HUVECs, cell membrane localization of DsRed-tagged β-arrestin 2 was induced by HDL-S1P but not by albumin- S1P (fig. S7). The ability of HDL to suppress the phosphorylation of p65 after TNFα treatment was blocked by short hairpin RNA (shRNA)–mediated knockdown of β-arrestin 2 but was not affected by overexpression of β-arrestin 2 (Fig. 6, B and C).

To confirm the involvement of $S1P_1$ in this response, HUVECs were treated with the $S1P_1$ inhibitor P-FTY720, which attenuated the ability of HDL-S1P to suppress TNFα-induced increases in ICAM-1 abundance (Fig. 6, D and E). These data suggest that a specific $ApoM^+$HDL-induced signaling complex consisting of $S1P_1$ and β-arrestin 2 was critical to inhibit cytokine-induced inflammatory responses.

Endothelial *S1pr1* abundance influences atherosclerosis development

Exaggerated inflammation in the vascular wall promotes atherosclerosis in the presence of hypercholesterolemia and hyperlipidemia (36). To determine the role of endothelial $S1P_1$ in atherosclerosis, we compared *Apoe*$^{-/-}$ *S1pr1ECKO* mice with *Apoe*$^{-/-}$ *S1pr1* wild-type littermates. As for *S1pr1ECKO* mice (Fig. 2C), ICAM-1 immunofluorescence was increased in *Apoe*$^{-/-}$ *S1pr1ECKO* mice, especially in the descending aorta (fig. S8).

When placed on a high-fat diet for 16 weeks, weight gain (fig. S9A) and plasma cholesterol concentrations (fig. S9B) were similar between *Apoe*$^{-/-}$ *S1pr1ECKO* and *Apoe*$^{-/-}$ *S1pr1* wild-type mice. In addition, monocyte ($CD11b^+$, $CD115^+$, $Ly6G^-$), neutrophil ($CD11b^+$, $Ly6C^{int}$, $Ly6G^{hi}$), T lymphocyte ($CD4^+$ and $CD8^+$), and B lymphocyte ($CD19^+$) numbers were similar in *Apoe*$^{-/-}$ *S1pr1ECKO* and *Apoe*$^{-/-}$ *S1pr1* wild-type mice (fig. S9, C and D). Also, plasma concentrations of ceramide and sphingosine species did not differ (fig. S10, A and B).

We next examined the development of atherosclerotic plaques using Oil Red O staining of en face preparations of the aorta (Fig. 7A). Quantification of plaque areas in the aortic arch (Fig. 7B) did not show significant differences. However, plaque development was significantly greater in the branch points of the descending aorta in *Apoe*$^{-/-}$ *S1pr1ECKO* mice than in *Apoe*$^{-/-}$ *S1pr1* wild-type mice, likely as a consequence of increased ICAM-1 and VCAM-1 abundance in this specific area (Fig. 7B and fig. S8). Consequently, total plaque area was significantly higher in the *Apoe*$^{-/-}$ *S1pr1ECKO* mice than in the *Apoe*$^{-/-}$

mice (Fig. 7B). Histological analysis of the lesions with hematoxylin-eosin, Masson's trichrome, or elastin staining indicated that plaque composition was similar in the two genotypes (fig. S11A). However, ICAM-1 staining was increased in plaques in *Apoe*$^{-/-}$ *S1pr1ECKO* animals (fig. S11B). Plaque areas in aortic roots (fig. S12, A and B) were similar in *Apoe*$^{-/-}$ *S1pr1ECKO* and *Apoe*$^{-/-}$ *S1pr1* wild-type mice. Although macrophage immunofluorescent staining in the aortic root did not appear to differ between the two genotypes (Fig. 7, C and D),more macrophage immunofluorescent signals were detected in plaques of the descending aorta in *Apoe*$^{-/-}$ *S1pr1ECKO* mice (Fig. 7, E and F). Together, these results suggest that endothelial $S1P_1$ exerts a region-specific antiatherosclerotic effect in the descending aorta.

DISCUSSION

Although sphingolipids, which function together with sterols in cellular membranes, are thought to be critical in cardiovascular disease, their specific functions in vascular pathophysiology remain unclear. S1P and its receptors are of particular interest, because the ligand is enriched in plasma, and the receptors are present on vascular and immune cells. Indeed, $S1P_2$ regulates myeloid cell retention in tissues during sterile inflammatory responses and in mouse models of atherosclerosis, and *S1pr2* knockout mice exhibit reduced atherosclerotic plaques (37, 38). In contrast, $S1P_1$ stimulation of monocytes-macrophages induces an anti-inflammatory phenotype (19), suggesting a potential function of S1P receptors in myeloid cells during vascular disease. However, despite its high abundance in the endothelium, the role of $S1P_1$ during vascular inflammation and atherosclerosis is still unknown.

A major finding of this work is that $S1P_1$ localization on the plasma membrane of aortic endothelial cells was inversely correlated with inflammatory adhesion molecule abundance. The surface amount of $S1P_1$ was substantially lower in endothelial cells of the lesser curvature, which are exposed to disturbed flow, than in those in the descending aorta. Analysis of the $S1P_1$-GFP reporter mice revealed that areas exposed to laminar shear did not show detectable $S1P_1$ signaling, whereas areas exposed to disturbed shear forces showed high signaling, which correlated with enhanced internalization of $S1P_1$ in these areas. Supraphysiological activation of $S1P_1$ results in enhanced endocytosis followed by degradation of the receptor (39, 40). The reason for this gradient of signaling, despite a uniform distribution of the ligand in the circulation, is not clear. A possible explanation for the enhanced signaling could be the increased permeability of disturbed shear areas of the endothelium (41), which would allow plasma S1P to access S1P receptors on the basolateral surface of the endothelium. Alternatively, disturbed shear stress per se or local inflammatory response could induce exaggerated $S1P_1$ signaling.

Endothelial $S1P_1$ signaling was analyzed with tissue-specific genetic loss of function and overexpression in mice. *S1pr1ECKO* mice showed increased VCAM-1 and ICAM-1 abundance, whereas mice that overexpressed *S1pr1* on endothelial cells had decreased abundance of these inflammatory markers in the aortic endothelium, suggesting that it suppressed inflammatory responses. In HUVECs, TNFα-induced NF-κB activation and adhesion molecule expression were suppressed by HDL-S1P, specifically

ApoM$^+$HDL.HDL-S1P induced the association of β-arrestin 2 with $S1P_1$ and promoted receptor localization on the plasma membrane, whereas S1P bound to albumin, its other chaperone in the plasma, suppressed forskolin-induced increases in cAMP concentrations. The ability of HDL-S1P to suppress inflammation depended on $S1P_1$, because P-FTY720 pretreatment, which triggers the degradation of $S1P_1$, antagonized it. However, both HDL-S1P and albumin- S1P activated the MAPK pathway in an $S1P_1$-dependent manner. Together, these data suggest that HDL-S1P acts as a biased agonist for $S1P_1$. The ability of specific chaperones to impart unique biological actions of S1P may be a general phenomenon, because we have described a unique function of HDL-S1P to suppress lymphopoiesis in the bone marrow (42). The mechanism underlying the differences in receptor activation by HDL-S1P and albumin-S1P is not known but could depend on co-receptors for HDL such as SR-B1 (25, 43).

Using defined HDL preparations (ApoM$^+$HDL and ApoM$^-$HDL), we showed that the association between $S1P_1$ and β-arrestin 2 correlated with the anti-inflammatory activity of HDL-S1P. In addition to the role of β-arrestins in the desensitization and internalization of GPCRs (33), they can act as G protein–independent signal transducers (44).For instance,β-arrestins can inhibit the proinflammatory cascade at different levels, by interacting either with inhibitor of nuclear factor κB α (IκBα) to enhance its stability (34, 35) or with the IκB kinase (IKK) complex directly (34). Moreover, studies on the receptor GPR120, which is activated by an ω-3 polyunsaturated fatty acid, showed that recruitment of β-arrestins (45) prevented downstream activation of the IKK complex and NF-κB activation. By using shRNA down-regulation in HUVECs, our data showed that β-arrestin 2 was essential for HDL-S1P to inhibit cytokine-induced inflammatory responses.

In the *Apoe*$^{-/-}$ background, *S1pr1ECKO* mice show enhanced plaque size, especially at branch points that are subject to disturbed shear stress and show exaggerated $S1P_1$ signaling. These mice did not show alterations in plasma cholesterol or sphingolipids, suggesting that attenuated signaling of the $S1P_1$ receptor in the endothelial compartment is responsible for the accelerated atherosclerosis. This suggests that endothelial $S1P_1$ protects the vessel wall from inflammation and atherosclerosis. These observations are consistent with findings that show that P-selectin–dependent leukocyte rolling is enhanced in postcapillary venules of $S1P_1$ endothelial knockout mice (46). In conclusion, our results highlight ApoM$^+$HDL chaperone– dependent anti-inflammatory and antiatherosclerotic function of S1P in the endothelium. This occurs through the activation of $S1P_1$, which transduces an anti-inflammatory signal in response to ApoM$^+$HDL-bound S1P. The ability of the S1P chaperone ApoM$^+$HDL to impart specific signal transduction mechanisms and an anti-inflammatory function in the endothelium may partially explain the cardiovascular protective functions of HDL.

MATERIALS AND METHODS

Mice

Animal experiments were approved by the Weill Cornell Medical College Institutional Animal Care and Use Committee. All experiments were done in male animals. *S1pr1*$^{f/f}$ mice were crossed to *Cdh5-Cre*^{ERT2} mice (a gift from R. Adams, Max Planck Institute) (47) to

generate *S1pr1*$^{f/f}$ *Cdh5-Cre*^{ERT2} mice. Gene deletion was achieved by intraperitoneal injection of tamoxifen (150 μg/day) to mice at 4 weeks of age for five consecutive days. For the atherosclerosis lesion development studies, *S1pr1*$^{f/f}$ *Cdh5-Cre*^{ERT2} mice were crossed with *Apoe*$^{-/-}$ mice (Jackson Laboratory) for >4 generations to obtain mice that were >95% C57Bl/6 background, as determined by single-nucleotide polymorphism analysis. *Apoe*$^{-/-}$ *S1pr1*$^{f/f}$ littermates (*Cdh5-Cre*^{ERT2}–negative) were used as controls. After $S1P_1$ deletion, male mice received high-fat chow (Teklad, TD88137; adjusted calories diet, 42% from fat) for 16 weeks.

S1pr1$^{f/stop/f}$ was generated as described (17) and crossed to *Cdh5-Cre*^{ERT2} mice to generate *S1pr1*$^{f/stop/f}$ *Cdh5-Cre*^{ERT2} mice. Gene overexpression was achieved by intraperitoneal injection of tamoxifen (150 μg/day) at 4 weeks of age for five consecutive days. *Apom*$^{-/-}$ mice were a gift of L. B. Nielsen and C. Christoffersen of Rigshospitalet. $S1P_1$-GFP reporter mice have been previously described (27).

Cell culture

HUVECs (passages 3 to 8) (Clonetics) were grown in MEM1999 supplemented with 10% heat-inactivated fetal bovine serum (FBS), 10 mM Hepes, heparin-stabilized, penicillin (50 μg/ml), streptomycin (50 μg/ml), and endothelial cell growth factor as previously described (48). GFP-tagged $S1P_1$ overexpression was done as previously described (49).

En face protocol and staining

After cervical dislocation, the superior vena cava was opened, and mice were flushed with cold phosphate-buffered saline (PBS) containing 5% heparin and a cocktail of phosphatase inhibitors (1 mM Na_3VO_4, 1 mM NaF, 10 mM β-glycerophosphate) followed by intracardiac injection of cold 4% paraformaldehyde (PFA) in PBS. Aortae were dissected and then fixed for 20 min in 4% PFA. After a brief wash in glycine solution (100 mM), followed by a10-min incubation in 0.1% Triton X-100, arteries were carefully opened, and descending aorta, lesser curvature, and greater curvature were isolated. Tissues were then incubated for 2 hours in blocking solution [75 mM NaCl, 18 mM Na_3 citrate, 2% FBS, 1% bovine serum albumin (BSA), 0.05% Triton X-100] as described previously (50), followed by incubation with primary antibodies diluted in blocking solution at 4°C under constant agitation.

After a 24-hour incubation with primary antibodies, arteries were washed for 2 hours in washing solution (75 mM NaCl, 18 mM Na_3 citrate, and 0.05% Triton X-100), incubated with fluorescent secondary antibodies (Alexa Fluor dyes, Molecular Probes) for 1 hour, counterstained with TO-PRO-3, mounted, and then imaged using an Olympus FluoView FV10i confocal microscope.

In vivo aortic protein biotinylation

Male age-matched mice were anesthetized with ketamine/xylene. The mice underwent thoracotomy, and an incision was made in the right ventricle. The left ventricle was perfused with cold PBS for 5 min and then by cell-impermeable Sulfo-NHS-Biotin (1 mg/ml) for 10min using an infusion pump (VWR) at a constant rate of 1 ml/min. Excess biotin was

rinsed out with consecutive 10-ml infusions of cold 50mMNH_4Cl in PBS followed by cold PBS alone. The thoracic aorta was harvested and immediately frozen in liquid nitrogen.

Immunoprecipitation

After the indicated treatments, HUVECs were washed in ice-cold PBS containing phosphatase inhibitors and lysed using modified radio-immunoprecipitation assay (RIPA) buffer [50 mM tris (pH 7.5), 150 mM NaCl, 1 mM EDTA, 1% NP-40, 0.5% sodium deoxycholate, 0.1% SDS, 1% Triton X-100, 0.5% FOS-choline, containing also 1 mM Na_3VO_4, 1 mMNaF, 10 mMβ-glycerophosphate, and protease inhibitor cocktail]. Lysates were then incubated for 20 min at 4°C using a tube rotator, and then centrifuged for 20 min at 13,500 rpm. Lysates were then cleared by protein A/G beads (Pierce Protein A Agarose, Thermo Scientific; Protein G Sepharose, GE Healthcare) and subjected to overnight immunoprecipitation using a monoclonal anti-$S1P_1$ immunoglobulin G antibody (H60, Santa Cruz Biotechnology). Bead-bound proteins were then separated on NuPAGE Novex 4 to 12% bis-tris gel (Invitrogen).

Cell surface biotinylation

After stimulation, cells were treated with a nonpermeable biotinylation agent (EZ-Link Sulfo-NHS-SS-Biotin) (Thermo Scientific) and lysed with a mild detergent following the supplier's protocol. Labeled proteins were then isolated using NeutrAvidin Agarose beads (Thermo Scientific) and subjected to Western blotting analysis.

Oil Red O staining of atherosclerotic plaques

Aortic lipid content was analyzed and quantified using Oil Red O staining, as described previously (51). Briefly, after CO_2 asphyxiation, aortae were harvested from heart to iliac bifurcation, opened in situ to expose the intima, and fixed in 4% PFA overnight. Lipids in plaques were stained using 0.5% Oil Red O solution. Once stained, aortae were digitally photographed, and plaque quantitation was performed using the Image-Pro Analyzer software. Aortic root lesion was determined as described before (38).

Monocyte/macrophage staining of atherosclerotic plaques

Cryosections of aortic root were incubated for 1 hour in blocking solution (75 mM NaCl, 18 mM Na_3 citrate, 2% FBS, 1% BSA, 0.05% Triton X-100) before immunostaining using rat anti-mouse MOMA-2 (Serotec). After incubation with fluorescent secondary antibody and nuclear counterstaining using DAPI (4′,6-diamidino-2-phenylindole) solution, sections were imaged using confocal microscope system (Olympus, FV10i).

Plasma cholesterol quantification

Cholesterol was quantified using Cholesterol E CHOD-DAOS method kit (Wako) according to the manufacturer's instructions. Results are expressed as microgram of cholesterol per deciliter of plasma.

Blood cell collection and flow cytometry

Mice were euthanized with CO_2 asphyxiation. Blood was recovered by hepatic portal vein puncture and collected in tubes containing 35 μl of 0.1 M EDTA. Whole blood (400 μl) was removed to a new tube, centrifuged at 2000*g* for 15 min, and plasma was removed and stored at −20°C. Cells were subjected to ammonium chloride erythrocyte lysis, washed with PBS, and stained with eFluor 718 fixable viability dye (eBioscience) according to the manufacturer's instructions. Cells were then briefly fixed for 30 min in 0.1% PFA, washed, and Fc receptors were blocked with TruStain FcX (BioLegend) in 5% FBS overnight at 4°C. Cells were then stained with the following antibody mixtures for 30 min on ice: CD4–phycoerythrin (PE) (RM4-4; BioLegend), CD8- PerCP/eFluor 710 (H35-17.2; eBioscience), CD19–eFluor 450 (ID3; eBioscience), CD11b–APC–eFluor 780 (M1/70; eBioscience), Ly6C–FITC (fluorescein isothiocyanate) (HK1.4; Southern Biotechnology), Ly6G-PECy7 (1A8; BioLegend), and CD115-APC (AFS98; BioLegend). Liquid counting beads (BD) were added to each sample, and data were obtained on a BD LSR II (Becton Dickson) and analyzed using FlowJo software (Tree Star Inc.).

HDL isolation

HDL_3 was isolated by fractionation of outdated pooled plasma (New York Blood Center) or freshly isolated mouse plasma from wild-type and *Apom*$^{-/-}$mice. Sequential ultracentrifugation, using increasing density solutions, was used to separate the different lipoprotein fractions according to their flotation (52). Endotoxin contamination was assessed using the Limulus assay (Enzo Life Science). Albumin contamination was analyzed by Western blotting, and only endotoxin-free, albumin-free HDL_3 isolations were used.

Immunoblot experiments

HUVECs were washed with cold PBS containing phosphate inhibitors (1 mM Na_3VO_4, 5mMNaF, and 10 mM β-glycerophosphate) and lysed with modified RIPA buffer [1 mM ETDA, 50 mM tris (pH 7.5), 150 mM NaCl, 1% NP-40, 0.5% sodium deoxycholate, 0.1% SDS, 1% Triton X-100, 0.5% FOS-choline] containing phosphatase inhibitors (1 mM Na_3VO_4, 1mMNaF, and 10mMβ-glycerophosphate) and protease inhibitor cocktail (Calbiochem). After a freeze/thaw cycle, lysates were sonicated, protein concentrations were determined by bicinchoninic acid assay (Pierce), and samples were briefly denatured at 95°C for 5 min after addition of 10% β-mercaptoethanol. Equal amounts of protein were separated into 10% polyacrylamide gel and transblotted on polyvinylidene difluoride membrane. Transferred proteins were then probed with the antibodies as indicated. Antibodies were obtained from Cell Signaling (pp65 NF-κB, β-arrestin 2, phospho P44-42 MAPK, and total ERK) or Santa Cruz Biotechnology ($S1P_1$, total p65 NF-κB, ICAM-1, and VCAM-1).

cAMP measurement

Cells were starved for 3 hours. Cells were then preincubated for 30 min with 1 mM IBMX (Tocris Bioscience) followed by stimulation for 30 min with albumin-S1P, $ApoM^-$ HDL, or $ApoM^+$HDL, in the presence of IBMX (1 mM) and forskolin (20 μM) (Tocris Bioscience). cAMP measurement was then assessed using the Direct cAMP ELISA (enzyme-linked immunosorbent assay) kit (Enzo Life Sciences) following the supplier's protocol.

Statistical analysis

Western blot quantification was done with ImageJ software (National Institutes of Health). Data are expressed as means ± SD. Statistical analysis was performed as mentioned using Prism software (Prism, GraphPad). *P* values <0.05 were considered significant.

Supplementary Material

Refer to Web version on PubMed Central for supplementary material.

Acknowledgments

We thank R. Adams, L. B. Nielsen, and C. Christoffersen for the gift of unique strains of mice. We also thank S. Narain and T. Prasad for their biostatistical advices and Kezhi Dai for help with the in vivo biotinylation assays.

Funding: This work was supported by NIH grants (PO1-HL70694 and RO1-HL89934 to T.H. and F32- CA142117 to V.A.B.). V.A.B. is a Leon Levy Research Fellow of the Weill Cornell Medical College Brain and Mind Research Institute. Sphingolipid measurements are supported in part by Lipidomics Shared Resource, Hollings Cancer Center, Medical University of South Carolina (P30 CA138313) and the Lipidomics Core in the South Carolina Lipidomics and Pathobiology Centers of Biomedical Research Excellence (COBRE) (P20 RR017677).

REFERENCES AND NOTES

1. Pober JS, Sessa WC. Evolving functions of endothelial cells in inflammation. Nat. Rev. Immunol. 2007; 7:803–815. [PubMed: 17893694]
2. Ley K, Laudanna C, Cybulsky MI, Nourshargh S. Getting to the site of inflammation: The leukocyte adhesion cascade updated. Nat. Rev. Immunol. 2007; 7:678–689. [PubMed: 17717539]
3. Nigro P, Abe J, Berk BC. Flow shear stress and atherosclerosis: A matter of site specificity. Antioxid. Redox Signal. 2011; 15:1405–1414. [PubMed: 21050140]
4. Barter P, Gotto AM, LaRosa JC, Maroni J, Szarek M, Grundy SM, Kastelein JJ, Bittner V, Fruchart JC. Treating to New Targets Investigators, HDL cholesterol, very low levels of LDL cholesterol, and cardiovascular events. N. Engl. J. Med. 2007; 357:1301–1310. [PubMed: 17898099]
5. Navab M, Ananthramaiah GM, Reddy ST, Van Lenten BJ, Ansell BJ, Fonarow GC, Vahabzadeh K, Hama S, Hough G, Kamranpour N, Berliner JA, Lusis AJ, Fogelman AM. The oxidation hypothesis of atherogenesis: The role of oxidized phospholipids and HDL. J. Lipid Res. 2004; 45:993–1007. [PubMed: 15060092]
6. Lusis AJ. Atherosclerosis. Nature. 2000; 407:233–241. [PubMed: 11001066]
7. Terasaka N, Yu S, Yvan-Charvet L, Wang N, Mzhavia N, Langlois R, Pagler T, Li R, Welch CL, Goldberg IJ, Tall AR. ABCG1 and HDL protect against endothelial dysfunction in mice fed a high-cholesterol diet. J. Clin. Invest. 2008; 118:3701–3713. [PubMed: 18924609]
8. Navab M, Reddy ST, Van Lenten BJ, Fogelman AM. HDL and cardiovascular disease: Atherogenic and atheroprotective mechanisms. Nat. Rev. Cardiol. 2011; 8:222–232. [PubMed: 21304474]
9. Rader DJ, Hovingh GK. HDL and cardiovascular disease. Lancet. 2014; 384:618–625. [PubMed: 25131981]
10. Nofer JR, van der Giet M, Tölle M, Wolinska I, von Wnuck Lipinski K, Baba HA, Tietge UJ, Gödecke A, Ishii I, Kleuser B, Schäfers M, Fobker M, Zidek W, Assmann G, Chun J, Levkau B. HDL induces NO-dependent vasorelaxation via the lysophospholipid receptor $S1P_3$. J. Clin. Invest. 2004; 113:569–581. [PubMed: 14966566]
11. Blaho VA, Hla T. Regulation of mammalian physiology, development, and disease by the sphingosine 1-phosphate and lysophosphatidic acid receptors. Chem. Rev. 2011; 111:6299–6320. [PubMed: 21939239]
12. Blaho VA, Hla T. An update on the biology of sphingosine 1-phosphate receptors. J. Lipid Res. 2014; 55:1596–1608. [PubMed: 24459205]

13. Schwab SR, Pereira JP, Matloubian M, Xu Y, Huang Y, Cyster JG. Lymphocyte sequestration through S1P lyase inhibition and disruption of S1P gradients. Science. 2005; 309:1735–1739. [PubMed: 16151014]

14. Christoffersen C, Obinata H, Kumaraswamy SB, Galvani S, Ahnström J, Sevvana M, Egerer-Sieber C, Muller YA, Hla T, Nielsen LB, Dahlbäck B. Endothelium-protective sphingosine-1-phosphate provided by HDL-associated apolipoprotein M. Proc. Natl. Acad. Sci. U.S.A. 2011; 108:9613–9618. [PubMed: 21606363]

15. Liu Y, Wada R, Yamashita T, Mi Y, Deng CX, Hobson JP, Rosenfeldt HM, Nava VE, Chae SS, Lee MJ, Liu CH, Hla T, Spiegel S, Proia RL. Edg-1, the G protein–coupled receptor for sphingosine-1-phosphate, is essential for vascular maturation. J. Clin. Invest. 2000; 106:951–961. [PubMed: 11032855]

16. Brinkmann V, Billich A, Baumruker T, Heining P, Schmouder R, Francis G, Aradhye S, Burtin P. Fingolimod (FTY720): Discovery and development of an oral drug to treat multiple sclerosis. Nat. Rev. Drug Discov. 2010; 9:883–897. [PubMed: 21031003]

17. Jung B, Obinata H, Galvani S, Mendelson K, Ding BS, Skoura A, Kinzel B, Brinkmann V, Rafii S, Evans T, Hla T. Flow-regulated endothelial S1P receptor-1 signaling sustains vascular development. Dev. Cell. 2012; 23:600–610. [PubMed: 22975328]

18. Whetzel AM, Bolick DT, Srinivasan S, Macdonald TL, Morris MA, Ley K, Hedrick CC. Sphingosine-1 phosphate prevents monocyte/endothelial interactions in type 1 diabetic NOD mice through activation of the S1P1 receptor. Circ. Res. 2006; 99:731–739. [PubMed: 16960101]

19. Hughes JE, Srinivasan S, Lynch KR, Proia RL, Ferdek P, Hedrick CC. Sphingosine- 1-phosphate induces an antiinflammatory phenotype in macrophages. Circ. Res. 2008; 102:950–958. [PubMed: 18323526]

20. Potì F, Gualtieri F, Sacchi S, Weißen-Plenz G, Varga G, Brodde M, Weber C, Simoni M, Nofer JR. KRP-203, sphingosine 1-phosphate receptor type 1 agonist, ameliorates atherosclerosis in LDL-R$^{-/-}$ mice. Arterioscler. Thromb. Vasc. Biol. 2013; 33:1505–1512. [PubMed: 23640484]

21. Nofer JR, Bot M, Brodde M, Taylor PJ, Salm P, Brinkmann V, van Berkel T, Assmann G, Biessen EA. FTY720, a synthetic sphingosine 1 phosphate analogue, inhibits development of atherosclerosis in low-density lipoprotein receptor–deficient mice. Circulation. 2007; 115:501–508. [PubMed: 17242282]

22. Keul P, Tölle M, Lucke S, vonWnuck Lipinski K, Heusch G, Schuchardt M, van der Giet M, Levkau B. The sphingosine-1-phosphate analogue FTY720 reduces atherosclerosis in apolipoprotein E–deficient mice. Arterioscler. Thromb. Vasc. Biol. 2007; 27:607–613. [PubMed: 17158351]

23. Kimura T, Tomura H, Mogi C, Kuwabara A, Ishiwara M, Shibasawa K, Sato K, Ohwada S, Im DS, Kurose H, Ishizuka T, Murakami M, Okajima F. Sphingosine 1-phosphate receptors mediate stimulatory and inhibitory signalings for expression of adhesion molecules in endothelial cells. Cell Signal. 2006; 18:841–850. [PubMed: 16111867]

24. Bolick DT, Srinivasan S, Kim KW, Hatley ME, Clemens JJ, Whetzel A, Ferger N, Macdonald TL, Davis MD, Tsao PS, Lynch KR, Hedrick CC. Sphingosine-1-phosphate prevents tumor necrosis factor-α-–mediated monocyte adhesion to aortic endothelium in mice. Arterioscler. Thromb. Vasc. Biol. 2005; 25:976–981. [PubMed: 15761190]

25. Kimura T, Tomura H, Mogi C, Kuwabara A, Damirin A, Ishizuka T, Sekiguchi A, Ishiwara M, Im DS, Sato K, Murakami M, Okajima F. Role of scavenger receptor class B type I and sphingosine 1-phosphate receptors in high density lipoprotein-induced inhibition of adhesion molecule expression in endothelial cells. J. Biol. Chem. 2006; 281:37457–37467. [PubMed: 17046831]

26. Fernández-Pisonero I, Dueñas AI, Barreiro O, Montero O, Sánchez-Madrid F, García-Rodriguez C. Lipopolysaccharide and sphingosine-1-phosphate cooperate to induce inflammatory molecules and leukocyte adhesion in endothelial cells. J. Immunol. 2012; 189:5402–5410. [PubMed: 23089395]

27. Kono M, Tucker AE, Tran J, Bergner JB, Turner EM, Proia RL. Sphingosine-1-phosphate receptor 1 reporter mice reveal receptor activation sites in vivo. J. Clin. Invest. 2014; 124:2076–2086. [PubMed: 24667638]

28. Baker RG, Hayden MS, Ghosh S. NF-κB, inflammation, and metabolic disease. Cell Metab. 2011; 13:11–22. [PubMed: 21195345]

29. Wilkerson BA, Grass GD, Wing SB, Argraves WS, Argraves KM. Sphingosine 1-phosphate (S1P) carrier-dependent regulation of endothelial barrier: High density lipoprotein (HDL)-S1P prolongs endothelial barrier enhancement as compared with albumin-S1P via effects on levels, trafficking, and signaling of S1P1. J. Biol. Chem. 2012; 287:44645–44653. [PubMed: 23135269]
30. Obinata H, Hla T. Sphingosine 1-phosphate in coagulation and inflammation. Semin. Immunopathol. 2012; 34:73–91. [PubMed: 21805322]
31. Goodman OB Jr, Krupnick JG, Santini F, Gurevich VV, Penn RB, Gagnon AW, Keen JH, Benovic JL. β-Arrestin acts as a clathrin adaptor in endocytosis of the β_2-adrenergic receptor. Nature. 1996; 383:447–450. [PubMed: 8837779]
32. Shenoy SK, Lefkowitz RJ. Seven-transmembrane receptor signaling through β-arrestin. Sci. STKE. 2005; 2005:cm10. [PubMed: 16267056]
33. Shenoy SK, Lefkowitz RJ. β-Arrestin-mediated receptor trafficking and signal transduction. Trends. Pharmacol. Sci. 2011; 32:521–533. [PubMed: 21680031]
34. Witherow DS, Garrison TR, Miller WE, Lefkowitz RJ. β-Arrestin inhibits NF-κB activity by means of its interaction with the NF-κB inhibitor IκBα. Proc. Natl. Acad. Sci. U.S.A. 2004; 101:8603–8607. [PubMed: 15173580]
35. Gao H, Sun Y, Wu Y, Luan B, Wang Y, Qu B, Pei G. Identification of β-arrestin2 as a G protein-coupled receptor-stimulated regulator of NF-κB pathways. Mol. Cell. 2004; 14:303–317. [PubMed: 15125834]
36. Libby P. Inflammation in atherosclerosis. Nature. 2002; 420:868–874. [PubMed: 12490960]
37. Michaud J, Im DS, Hla T. Inhibitory role of sphingosine 1-phosphate receptor 2 in macrophage recruitment during inflammation. J. Immunol. 2010; 184:1475–1483. [PubMed: 20042570]
38. Skoura A, Michaud J, Im DS, Thangada S, Xiong Y, Smith JD, Hla T. Sphingosine- 1-phosphate receptor-2 function in myeloid cells regulates vascular inflammation and atherosclerosis. Arterioscler. Thromb. Vasc. Biol. 2011; 31:81–85. [PubMed: 20947824]
39. Oo ML, Chang SH, Thangada S, Wu MT, Rezaul K, Blaho V, Hwang SI, Han DK, Hla T. Engagement of $S1P_1$-degradative mechanisms leads to vascular leak in mice. J. Clin. Invest. 2011; 121:2290–2300. [PubMed: 21555855]
40. Liu CH, Thangada S, Lee MJ, Van Brocklyn JR, Spiegel S, Hla T. Ligand-induced trafficking of the sphingosine-1-phosphate receptor EDG-1. Mol. Biol. Cell. 1999; 10:1179–1190. [PubMed: 10198065]
41. Orr AW, Stockton R, Simmers MB, Sanders JM, Sarembock IJ, Blackman BR, Schwartz MA. Matrix-specific p21-activated kinase activation regulates vascular permeability in atherogenesis. J. Cell Biol. 2007; 176:719–727. [PubMed: 17312022]
42. Blaho VA, Galvani S, Engelbrecht E, Liu C, Swendeman SL, Kono M, Proia RL, Steinman L, Han MH, Hla T. HDL-bound sphingosine-1-phosphate restrains lymphopoiesis and neuroinflammation. Nature. 2015; 523:342–346. [PubMed: 26053123]
43. Yuhanna IS, Zhu Y, Cox BE, Hahner LD, Osborne-Lawrence S, Lu P, Marcel YL, Anderson RG, Mendelsohn ME, Hobbs HH, Shaul PW. High-density lipoprotein binding to scavenger receptor-BI activates endothelial nitric oxide synthase. Nat. Med. 2001; 7:853–857. [PubMed: 11433352]
44. DeWire SM, Ahn S, Lefkowitz RJ, Shenoy SK. β-Arrestins and cell signaling. Annu. Rev. Physiol. 2007; 69:483–510. [PubMed: 17305471]
45. Oh DY, Talukdar S, Bae EJ, Imamura T, Morinaga H, Fan W, Li P, Lu WJ, Watkins SM, Olefsky JM. GPR120 is an omega-3 fatty acid receptor mediating potent anti-inflammatory and insulin-sensitizing effects. Cell. 2010; 142:687–698. [PubMed: 20813258]
46. Nussbaum C, Bannenberg S, Keul P, Gräler MH, Gonçalves-de-Albuquerque CF, Korhonen H, von Wnuck Lipinski K, Heusch G, de Castro Faria Neto HC, Rohwedder I, Göthert JR, Prasad VP, Haufe G, Lange-Sperandio B, Offermanns S, Sperandio M, Levkau B. Sphingosine-1-phosphate receptor 3 promotes leukocyte rolling by mobilizing endothelial P-selectin. Nat. Commun. 2015; 6:6416. [PubMed: 25832730]
47. Pitulescu ME. I. Schmidt, R. Benedito, R. H. Adams, Inducible gene targeting in the neonatal vasculature and analysis of retinal angiogenesis in mice. Nat. Protoc. 2010; 5:1518–1534. [PubMed: 20725067]

48. Hla T, Maciag T. An abundant transcript induced in differentiating human endothelial cells encodes a polypeptide with structural similarities to G-protein-coupled receptors. J. Biol. Chem. 1990; 265:9308–9313. [PubMed: 2160972]

49. Obinata H, Gutkind S, Stitham J, Okuno T, Yokomizo T, Hwa J, Hla T. Individual variation of human $S1P_1$ coding sequence leads to heterogeneity in receptor function and drug interactions. J. Lipid. Res. 2014; 55:2665–2675. [PubMed: 25293589]

50. Filipe C, Lam Shang Leen L, Brouchet L, Billon A, Benouaich V, Fontaine V, Gourdy P, Lenfant F, Arnal JF, Gadeau AP, Laurell H. Estradiol accelerates endothelial healing through the retrograde commitment of uninjured endothelium. Am. J. Physiol. Heart Circ. Physiol. 2008; 294:H2822–H2830. [PubMed: 18441207]

51. Maganto-Garcia E, Tarrio M, Lichtman AH. Mouse models of atherosclerosis. Curr. Protoc. Immunol. 2012; 96:15.24.1–15.24.23.

52. Hatch FT. Practical methods for plasma lipoprotein analysis. Adv. Lipid Res. 1968; 6:1–68. [PubMed: 4179999]

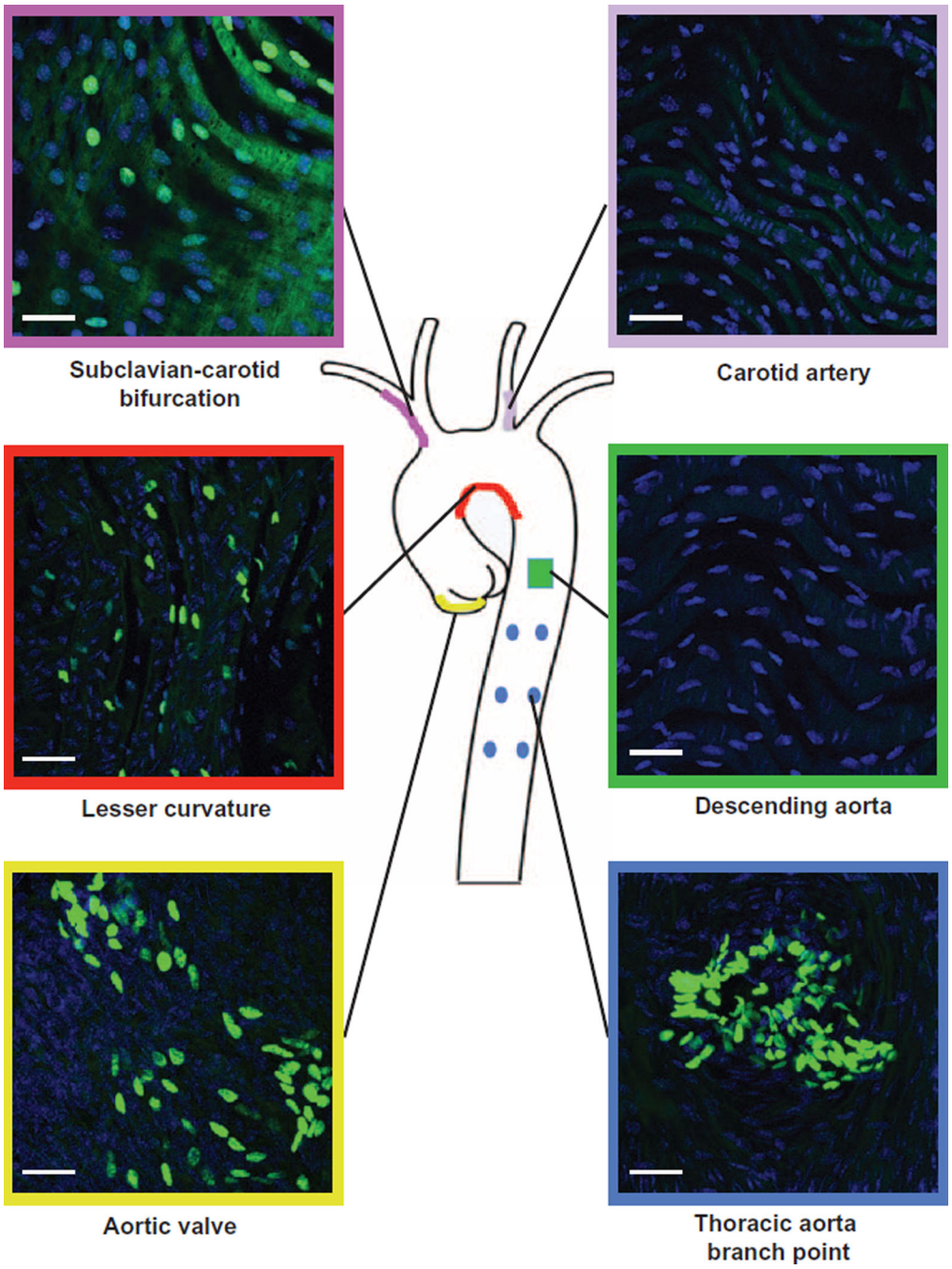

Fig. 1. $S1P_1$ activation in the aortic endothelium exposed to disturbed shear forces

Aortae from $S1P_1$-GFP signaling mice (27) were dissected, and nuclei were counterstained in en face preparations. Nuclear GFP abundance was analyzed by immunofluorescence in aortic valve (yellow lining), lesser curvature (red lining), subclavian-carotid bifurcation (purple lining), carotid artery (pink lining), descending aorta (green lining), and thoracic aorta branch point (blue lining). Images are representative of eight mice obtained in five independent experiments.

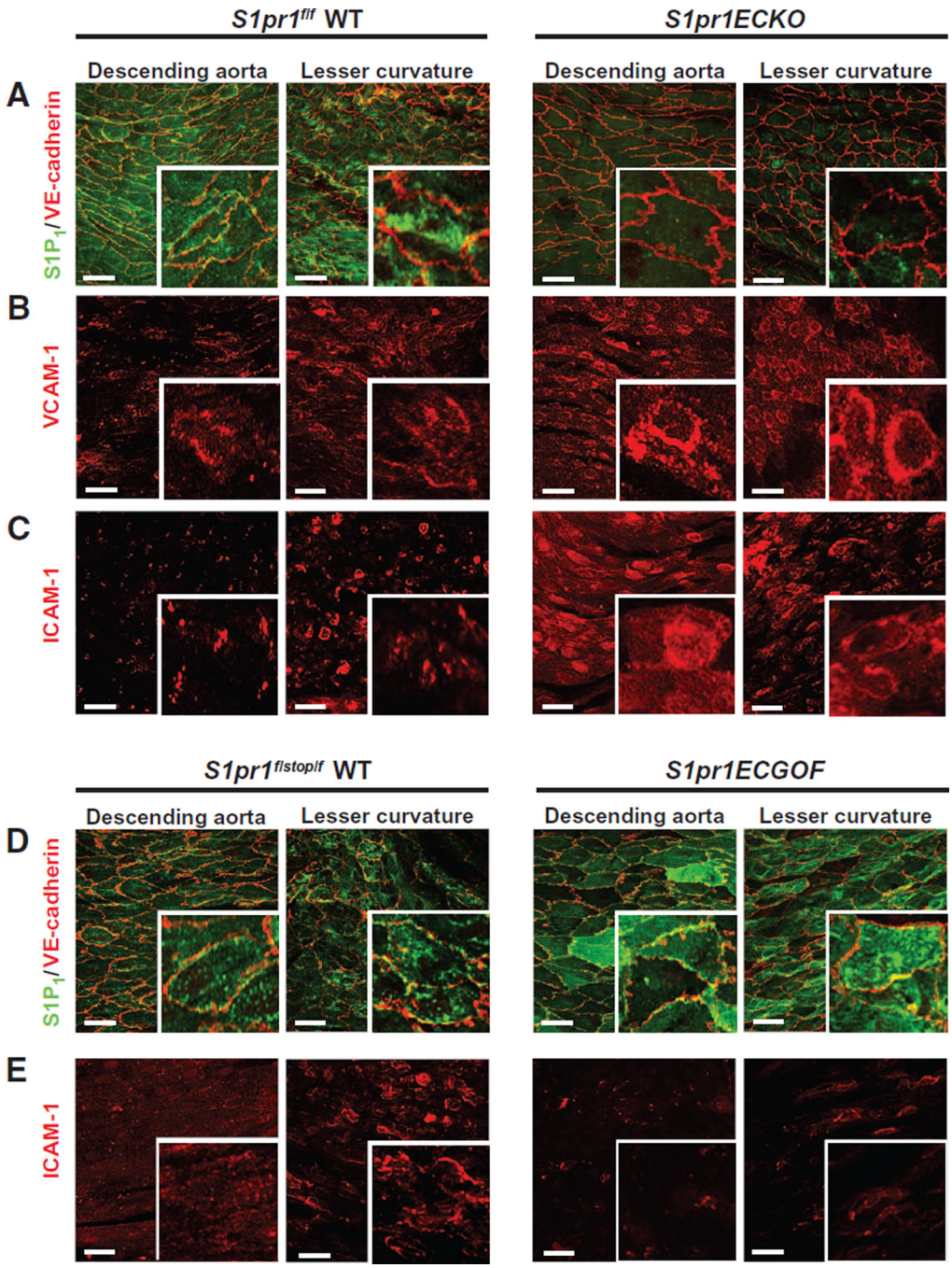

Fig. 2. Genetic modulation of endothelial $S1P_1$ expression and inflammatory marker expression

Aortae from wild-type (WT) (*S1pr1*$^{f/f}$) and *S1pr1ECKO* (*S1pr1*$^{f/f}$ *Cdh5-Cre*$^{ERT2+/-}$) mice were dissected, and intima was stained in en face preparations. (**A**) Immunostaining of $S1P_1$ and VE-cadherin. $S1P_1$ immunofluorescence was undetectable in *S1pr1ECKO* aortae. (**B** and **C**) Immunostaining for VCAM-1 (B) and ICAM-1 (C) in the presence or absence of endothelial $S1P_1$. Images are representative of 10 mice per genotype obtained in 8 to 10 independent experiments. Aortae from WT (*S1pr1*$^{f/stop/f}$) and *S1pr1ECGOF* (*S1pr1*$^{f/stop/f}$ *Cdh5-Cre*$^{ERT2+/-}$) mice were dissected, and intima was stained in en face preparations. (**D**)

Immunostaining of $S1P_1$ and VE-cadherin. $S1P_1$ immunofluorescence was increased in *S1pr1ECGOF* aortae. (**E**) Immunostaining for ICAM-1 with and without endothelial $S1P_1$ overexpression. Images are representative of 10 mice per genotype obtained in five to seven independent experiments.

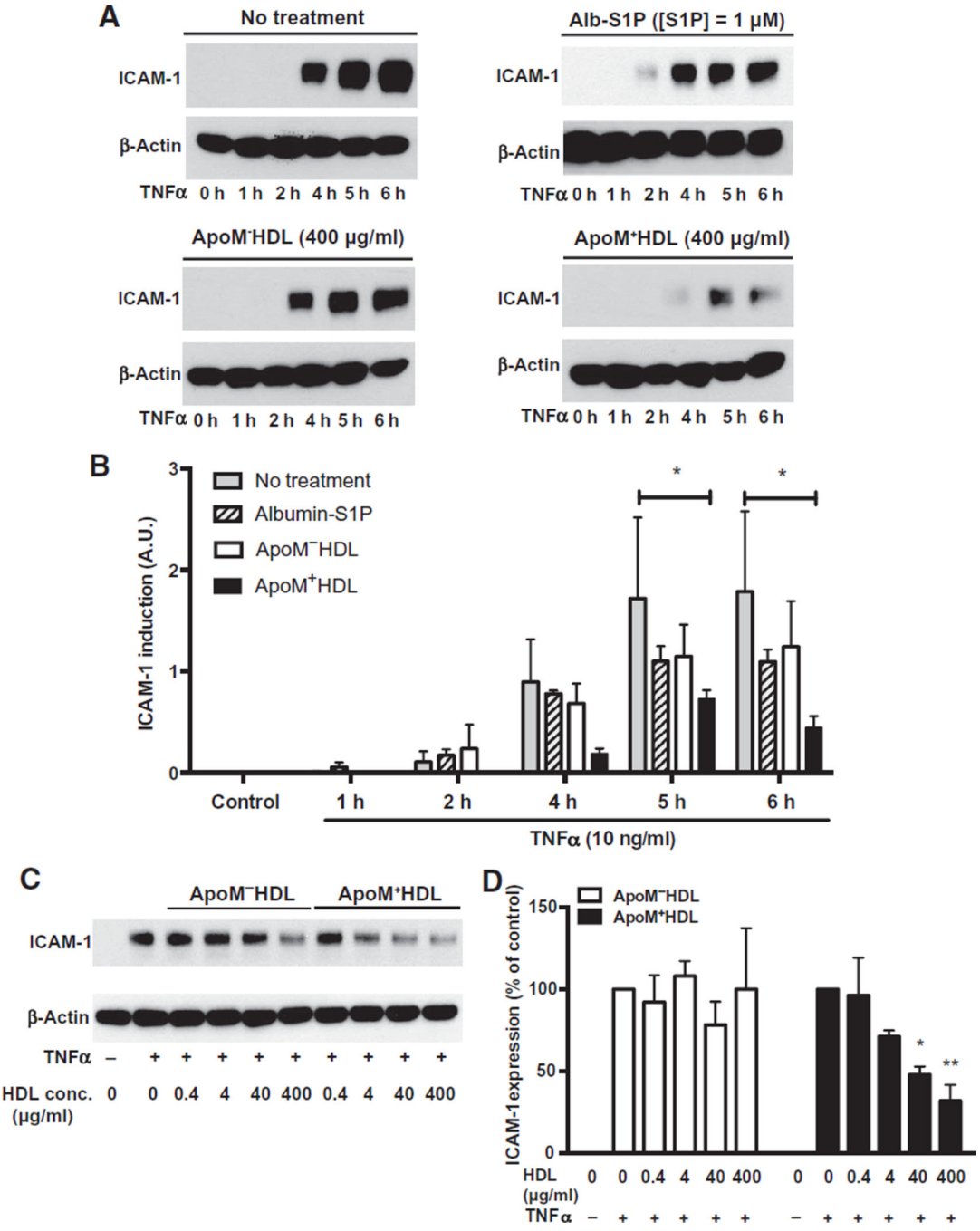

Fig. 3. S1P chaperone–dependent inhibition of TNFα-induced increase in ICAM-1 abundance

(**A**) Serum-starved HUVECs were stimulated with human recombinant TNFα for the indicated times, in the absence or presence of HDL isolated from WT (ApoM$^+$HDL) or *Apom*$^{-/-}$ (ApoM$^-$HDL) mice or albumin (Alb)–S1P. ICAM-1 abundance was assessed by immunoblot of total cell lysates. (**B**) ICAM-1 abundance was quantified from three independent experiments. Data are shown as means ± SD. **P* < 0.05 by two-way analysis of variance (ANOVA) followed by Dunnett's multiple comparison (no treatment compared to each treatment for every time point). A.U., arbitrary unit. (**C**) Serum-starved HUVECs were

stimulated with human recombinant TNFα and with increasing doses of ApoM^{-}HDL or ApoM^{+}HDL as indicated. ICAM-1 abundance was determined by immunoblot analysis. (**D**) Data are shown as means ICAM abundance ± SD from three independent experiments. *P < 0.05, compared to TNFα alone by Kruskal Wallis test followed by Dunnett's multiple comparison.

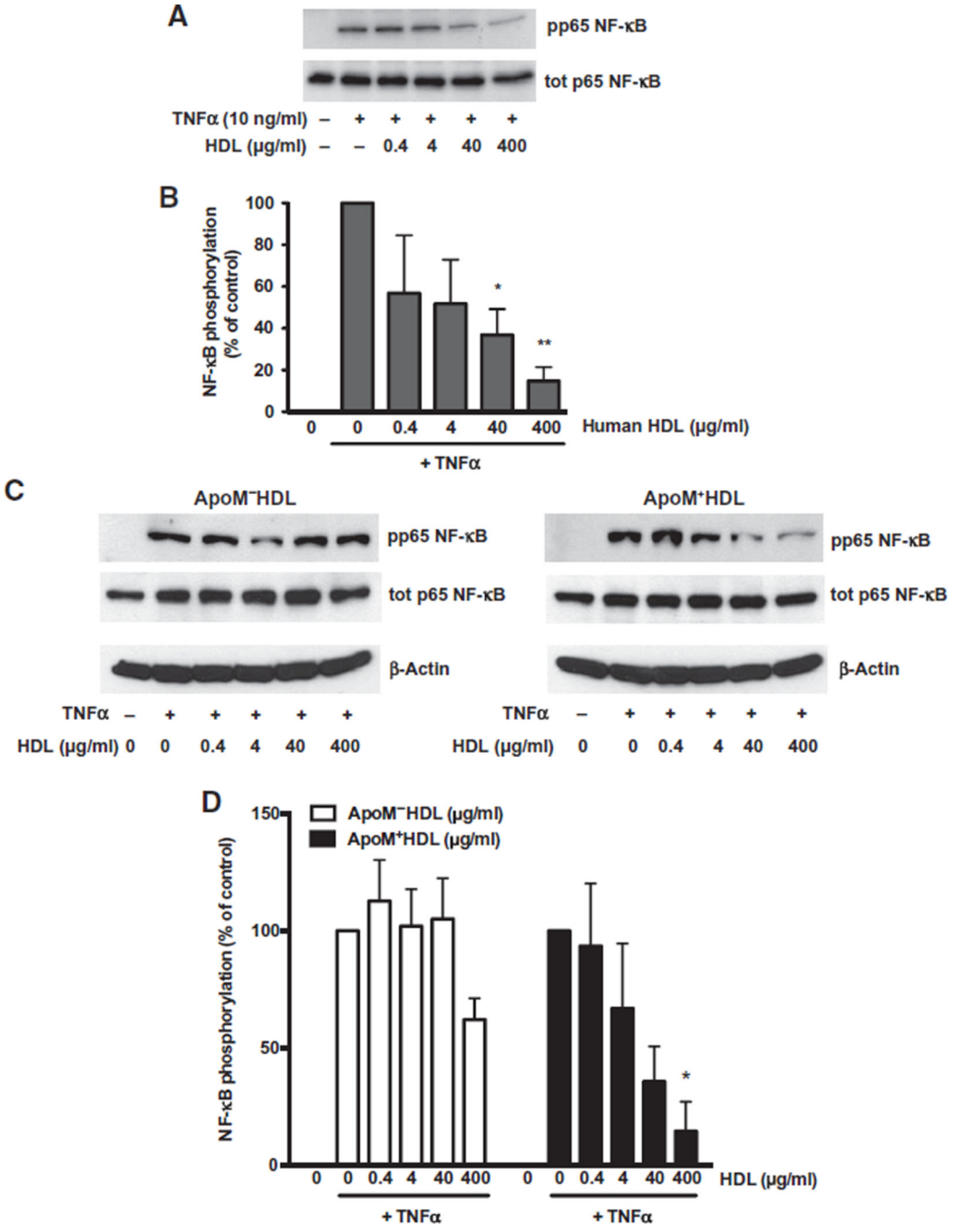

Fig. 4. HDL-S1P suppresses cytokine-induced NF-κB activation

(**A** and **C**) Serum-starved HUVECs were stimulated with TNFα with or without increasing doses of human HDL (A) or WT mouse HDL (ApoM$^+$HDL) and mouse HDL from *Apom*$^{-/-}$ animals (ApoM$^-$HDL) (C). Phosphorylation (p) of the NF-κB subunit p65 was analyzed by immunoblot of total (tot) cell lysates. (**B** and **D**) Data in (B) and (D) represent combined analysis from three independent experiments and are shown as means ± SD. **P* < 0.05, ***P* < 0.01, compared to TNFα alone by one-way ANOVA followed by Dunnett's multiple comparison.

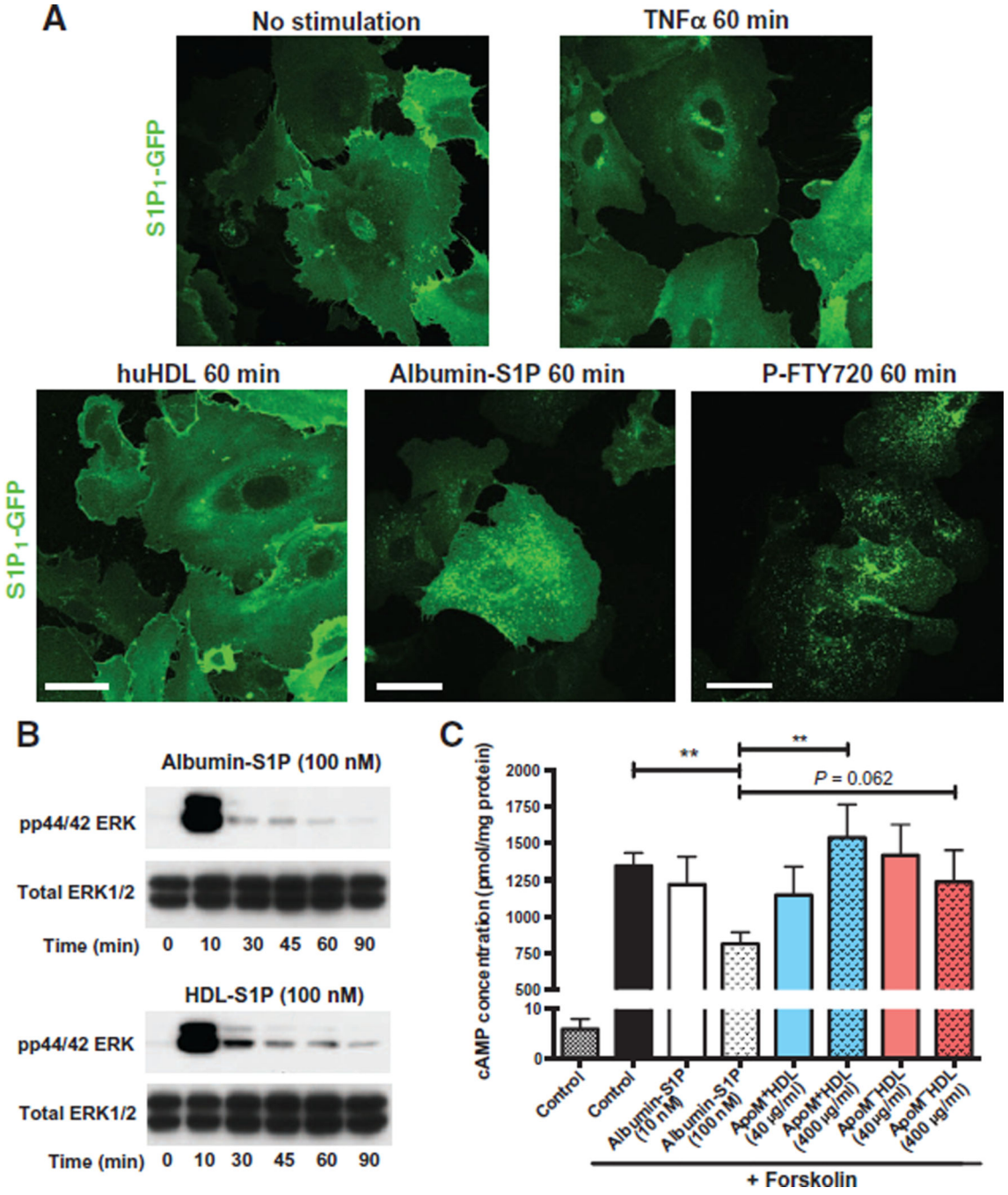

Fig. 5. HDL-S1P acts as a biased agonist on $S1P_1$

(**A**) HUVECs were transduced with lentivirus encoding GFP-tagged $S1P_1$ and after serum starvation, were stimulated with TNFα or with human HDL (huHDL), albumin- S1P, or P-FTY720 for the indicated times. Confocal microscopy was performed to assess the localization of GFP-tagged $S1P_1$. Images are representative of three independent experiments. (**B**) Serum-starved HUVECs were stimulated with albumin-S1P or HDL-S1P for the indicated times. MAPK phosphorylation was assessed by immunoblot of total lysates. (**C**) Serum-starved HUVECs were preincubated for 30 min with 3-isobutyl-1-

methylxanthine (IBMX), and then stimulated with increasing doses of albumin-S1P, HDL-S1P, or ApoM^{-}HDL in the presence of forskolin for 30 min. Results are expressed as picomole of cAMP per microgram of protein. Data represent combined analysis of five separate experiments and are expressed as means ± SD. $^{**}P < 0.01$ by Friedman test followed by Dunnett's multiple comparisons.

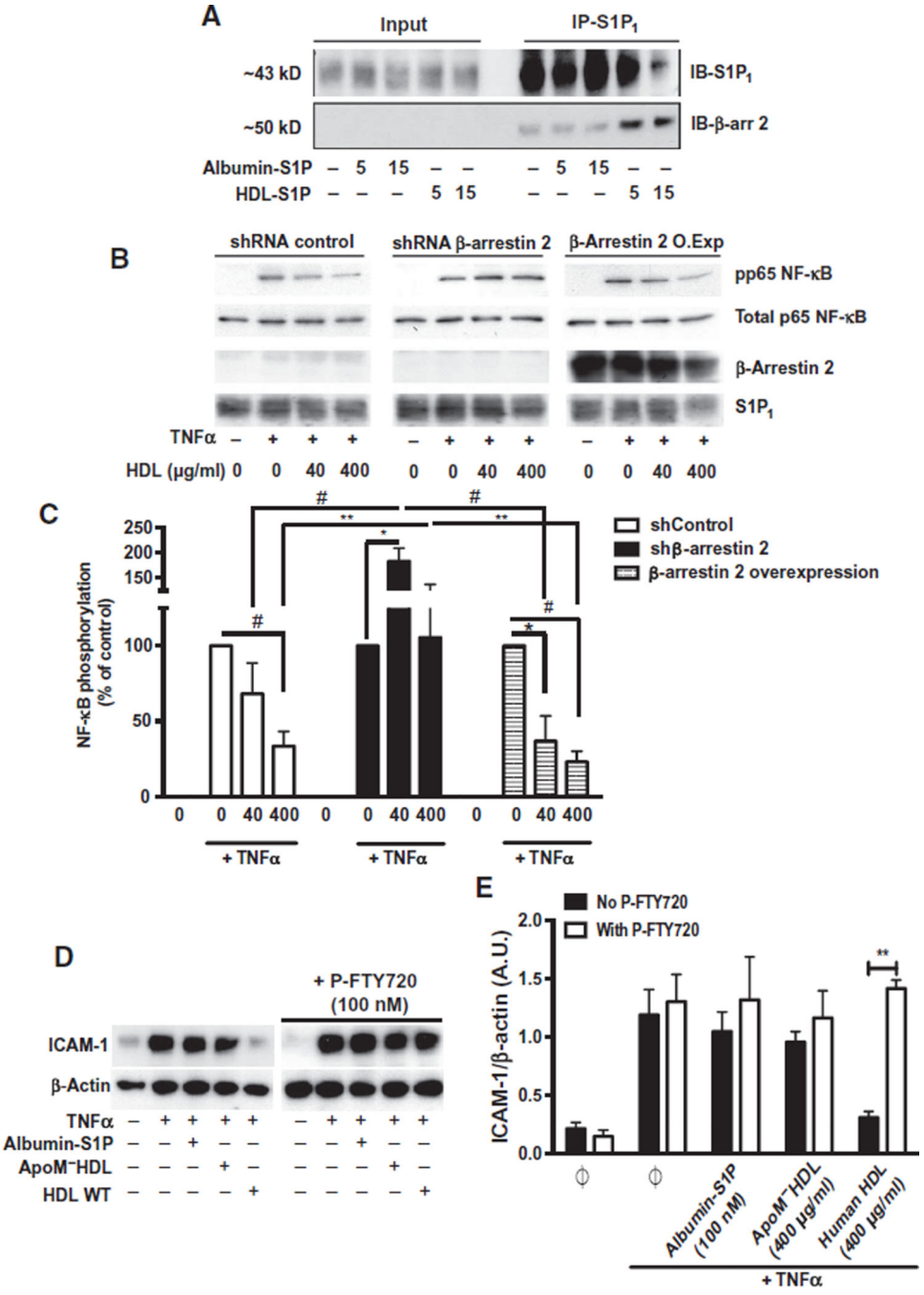

Fig. 6. The role of β-arrestin 2 in the biased signaling of HDL-S1P

(**A**) Serum-starved HUVECs were treated with albumin-S1P or human HDL-S1P for the indicated times. Cell lysates were subjected to immunoprecipitation for $S1P_1$ and immunoblotted (IB) with β-arrestin 2 antibody. Immunoblots are representative of three independent experiments. (**B**) HUVECs stably overexpressing β-arrestin 2 complementary DNA or an shRNA directed against β-arrestin 2 were serum-starved and stimulated with TNFα, with or without human HDL at the indicated doses. p65 phosphorylation was analyzed by immunoblot assay. (**C**) Data represent combined analysis of p65

phosphorylation from four independent experiments. *$P < 0.05$, **$P < 0.01$, $^{\#}P < 0.005$ by two-way ANOVA followed by Dunnett's multiple comparison. (**D**) Serum-starved HUVECs were stimulated with TNFα in the absence or presence of albumin-S1P or ApoM^{-}HDL or human HDL as indicated. In the P-FTY720–treated experiments, serum-starved HUVECs were pretreated with P-FTY720 in the absence or presence of albumin-S1P, ApoM^{-}HDL, or human HDL before TNFα stimulation in the presence of P-FTY720. ICAM-1 abundance was assessed by immunoblotting. (**E**) Data represent the combined analysis of ICAM-1 abundance from three independent experiments. **$P < 0.01$ by unpaired Student's *t* test.

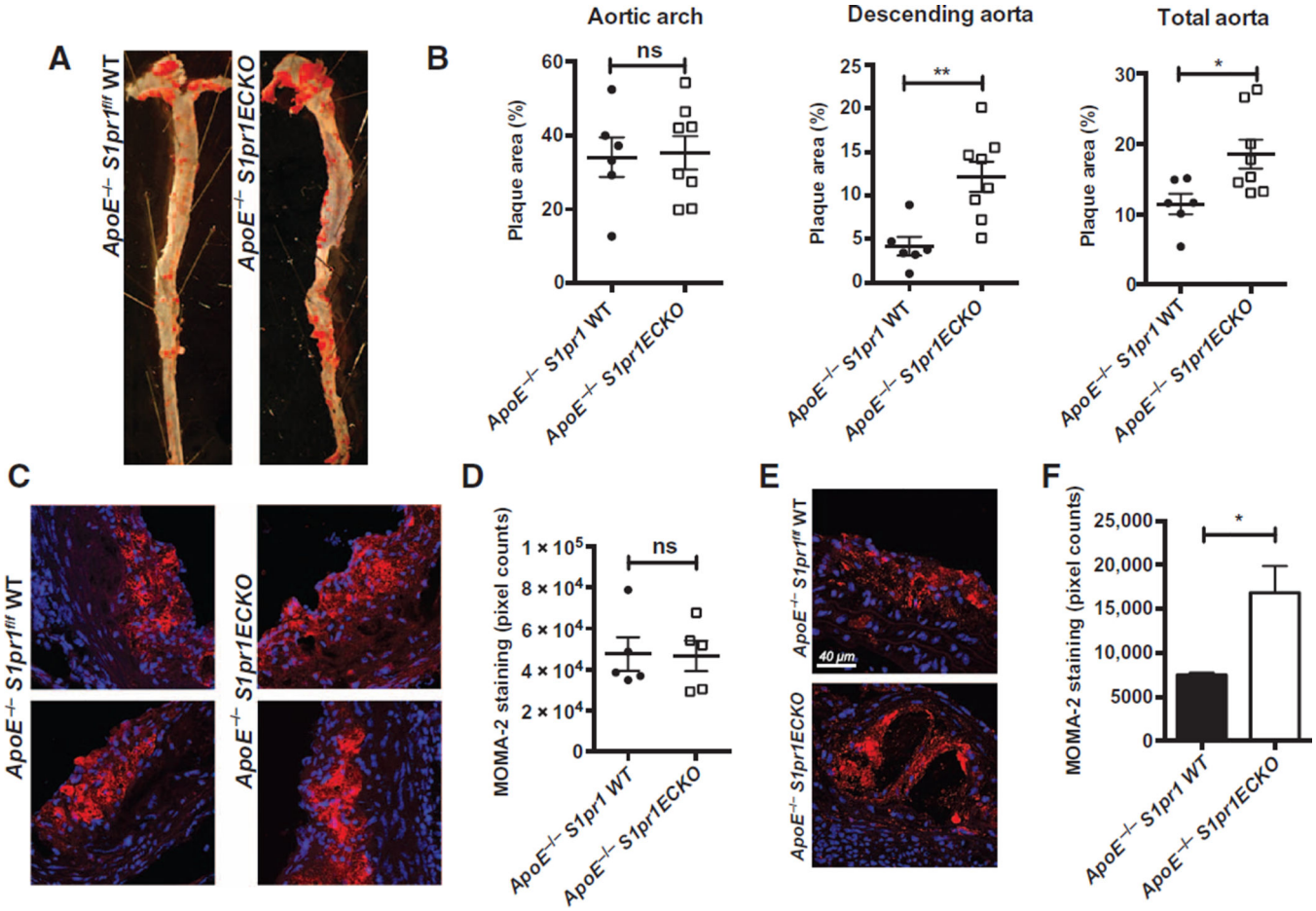

Fig. 7. Endothelial $S1P_1$ suppresses atherosclerotic lesion development

Male *Apoe*$^{-/-}$ *S1pr1 WT* and *Apoe*$^{-/-}$ *S1pr1ECKO* littermates were placed on high-fat diet for 16 weeks. (**A**) Aortae were dissected; en face preparation followed by Oil Red O staining was done. Shown here is a representative image of aorta from each group. (**B**) Quantification of plaque areas in each section of aorta (aortic arch, descending aorta, and total aorta) is shown (six *Apoe*$^{-/-}$ *WT* mice and eight *Apoe*$^{-/-}$ *S1pr1ECKO* mice). ns, not significant. (**C**) Aortic root sections from *Apoe*$^{-/-}$ *S1pr1 WT* and *Apoe*$^{-/-}$ *S1pr1ECKO* mice were immunostained with MOMA-2 to visualize the infiltration of macrophages and foam cells. (**D**) Quantification of MOMA-2 infiltration in the aortic valve was assessed ($n = 5$ mice for each genotype). (**E**) Plaques from descending aorta of *Apoe*$^{-/-}$ *S1pr1 WT* and *Apoe*$^{-/-}$ *S1pr1ECKO* mice were isolated, and macrophage was visualized by MOMA-2 staining followed by confocal microscopy. (**F**) Quantification of MOMA-2 staining in the descending aorta lesion was assessed ($n = 2$ animals, two separate plaques analyzed for each aorta). Data are shown as means ± SD. *$P < 0.05$, **$P < 0.01$ by Mann-Whitney test.